Detuning Analysis and Design Optimization of an 1.3 GHz 3-cell Superconducting Cavity

Xinghao Guo,[1,2] Xia Yan,[2] Yawei Huang,[2] Xuan Huang,[3] Xiaoyun Pu,[1]
Xiaowei Wu,[4,*] Jinfang Chen,[1,†] Dong Wang,[1] Liang Chu,[3] and Haixiao Deng[1]

[1]*Shanghai Advanced Research Institute, Chinese Academy of Sciences, Shanghai 201210, China*
[2]*ShanghaiTech University, Shanghai 201210, China*
[3]*Shanghai Institute of Applied Physics, Chinese Academy of Sciences, Shanghai 201800, China*
[4]*Zhangjiang Laboratory, Shanghai 201210, China*

Energy recovery linac (ERL) offers a promising path to superior beam quality and substantial energy savings at high average beam currents. This paper concentrates on optimizing the structure of a 1.3 GHz 3-cell superconducting cavity for high-current ERL injectors. It particularly examines helium pressure sensitivity and the detuning mechanism in the cavity. To mitigate detuning, strategies such as optimizing stiffening rings, reducing the helium vessel diameter, and enhancing cavity stiffness are proposed. Additionally, the paper outlines the mechanical design of the cavity and evaluates its performance through tuning force, Lorentz force detuning, stress, and modal analyses to ensure robustness and reliability.

Keywords: Energy Recovery Linac, High-Current Superconducting Cavity, Detuning, Stiffening Rings, Microphonics

I. INTRODUCTION

The core concept of Energy Recovery Linac (ERL) is that, after initial acceleration, the electron beam emits high-brightness radiation, while a specially designed loop guides it back to the accelerating section in a decelerated state. This process recovers the electron beam's kinetic energy, converting it into high-frequency electromagnetic waves, which are then used to accelerate new electron beams, while the decelerated old beam is discarded. This design significantly reduces energy consumption and ensures the quality of the electron beam, making ERL an effective method for generating high quality electron beams[1]. ERL projects worldwide have demonstrated remarkable advancements in beam energy recovery and operational efficiency. The CEBAF experiment achieved a maximum energy of $1055\,\mathrm{MeV}$ in single-pass configurations with a continuous-wave (CW) beam current of $80\,\mu\mathrm{A}$[2, 3]. The CBETA project demonstrated multi-turn energy recovery using superconducting radio-frequency (SRF) cavities and a fixed-field alternating-gradient (FFAG) system. The permanent magnets are arranged in the FFAG system to construct a single return loop that successfully transports electron bunches of 42, 78, 114, and $150\,\mathrm{MeV}$ in one common vacuum chamber[4, 5]. The cERL facility at KEK has successfully demonstrated stable CW operation at 1 mA with beam energies ranging from 17.6 to $20\,\mathrm{MeV}$, achieving energy recovery efficiency exceeding 99.9%[6, 7]. The recirculating superconducting linear accelerator S-DALINAC at TU Darmstadt's Institute for Nuclear Physics is a key research tool. It operates in CW mode, achieving beam currents up to $20\,\mu\mathrm{A}$ and energies as high as $130\,\mathrm{MeV}$, employing a three-pass recirculation scheme[8]. Future projects such as MESA at Mainz University in Germany, PERLE at IJC in France, the five-pass CEBAF at JLAB, and the EIC Cooler at Brookhaven National Laboratory in the U.S. will all rely on high-current SRF accelerator technologies due to their ability to achieve high beam intensities, efficient energy recovery, and stable continuous-wave operation[9–12]. Together, these projects underscore the transformative potential of ERL technology in achieving high-energy efficiency and beam quality. Based on the recent developments of the continuous-wave SRF accelerator technology[13–19], the project of this paper also investigates ERL-based linear accelerators and proposes a concept to achieve an average operational beam current of $10\,\mathrm{mA}$. This study presents an in-depth analysis and optimization of the mechanical structure of an $1.3\,\mathrm{GHz}$ high-current injector SRF cavity, significantly enhancing its frequency stability and mechanical performance. Additionally, a comprehensive simulation methodology for evaluating the stability and strength of SRF cavities has been developed. This methodology establishes a solid theoretical foundation for future cavity manufacturing and tuning processes, providing valuable engineering insights for research.

To meet the $10\,\mathrm{mA}$ average beam current requirement of the ERL project, a complete radio-frequency (RF) parameter design of the injector cavity was implemented and an $1.3\,\mathrm{GHz}$ 3-cell injector superconducting cavity configuration was selected[20, 21]. The vacuum model of the SRF cavity is shown in Fig. 1. This study focuses on the design and performance evaluation of an $1.3\,\mathrm{GHz}$ 3-cell injector superconducting cavity for an energy recovery linac aimed at achieving an average current of 10 mA. Based on the physical design, the mechanical structure of the high-current $1.3\,\mathrm{GHz}$ SRF cavity was designed and evaluated, with emphasis on key parameters such as mechanical strength, helium pressure detuning, Lorentz detuning, and modal analysis. A multiphysics optimization approach was applied to the cavity, with particular attention given to detuning and stability. Finite element simulation software was used to optimize and reinforce the cavity structure which is crucial for the fabrication of high-current SRF cavities. Through design optimization, the cavity's frequency and phase deviations caused by small deformations during operation were effectively controlled. This research

* Corresponding author, Xiaowei Wu, Zhangjiang Laboratory, Shanghai 201210, China, wuxw@zjlab.ac.cn

† Corresponding author, Jinfang Chen, Shanghai Advanced Research Institute, Chinese Academy of Sciences, Shanghai 201210, Chinac, chenjinfang@sari.ac.cn

provides valuable insights into the mechanical properties of SRF cavities and offers important theoretical support for the fabrication process.

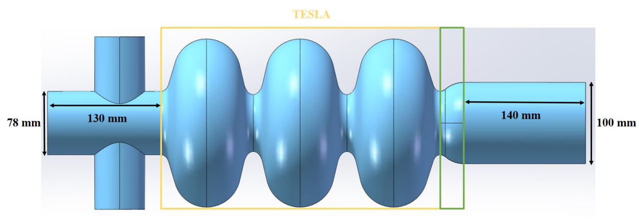

Fig. 1. Vacuum model of the 1.3 GHz 3-cell SRF injector cavity. The green area represents the designed transition section. The yellow area maintains the same mid-cell and end-cell dimensions as the TESLA cavity.

Chapter II details the theoretical framework of key detuning mechanisms in superconducting cavities, establishing a foundation for subsequent analysis. Chapter III conducts a systematic investigation of helium pressure sensitivity (df/dp) across different tuner stiffness configurations, with the study specifically aimed at quantifying the cavity's mechanical response to pressure fluctuations. This analysis utilizes multiphysics-coupled finite element simulations to correlate structural deformations with frequency detuning, providing critical insights into the cavity's stability. Chapter IV systematically formulates the primary factors contributing to cavity detuning, quantifies their individual effects, and validates the results through comparisons with full-model simulations. Chapter V focuses on the mechanical design of the cavity, covering the evaluation of tuning forces and Lorentz force detuning, and concludes with a thorough assessment of the cavity's structural strength to ensure its operational reliability.

II. DETUNING THEORY OF SUPERCONDUCTING CAVITY

A. Microphonics

Superconducting cavities are typically designed with thin walls, usually less than 3 mm[22], to meet heat dissipation and tuning requirements. This design makes them highly susceptible to deformation from external disturbances. Mechanical resonance occurs when the frequency of external vibrations closely matches the natural mechanical resonance frequency of the cavity. This phenomenon, termed microphonics, leads to substantial structural deformation and frequency instability. External sources of vibration, including ambient noise, equipment operation, and structural vibrations, are the primary causes of this effect.

To mitigate the impact of external vibrations on high-frequency superconducting cavities and prevent resonance, three strategies are commonly used: the first involves adding vibration isolation systems to reduce the transmission of environmental vibrations, the second utilizes low-level control compensation to counteract vibrations, and the third optimizes the cavity's mechanical design to increase its natural mechanical resonance frequency, reducing its susceptibility to resonance[23]. The first two methods focus on optimizing the external environment and active control. And this paper focuses on the third approach, improving the cavity's structural design to improve its natural machanical resonance frequency.

During the design phase, analyzing the mechanical vibration modes of the cavity helps to identify its natural mechanical frequencies. External vibrations are typically below 50 Hz and have relatively large amplitudes. As a result, the low-frequency modes within the superconducting cavity are more likely to resonate with environmental vibration sources. Increasing the cavity's mechanical resonance frequency minimizes the risk of resonance with low-frequency environmental vibrations, reducing microphone detuning effects.

B. Helium pressure fluctuation

In superconducting accelerator systems, the liquid helium tank plays a crucial role in maintaining the low-temperature operating state of the superconducting cavity. Fluctuations and pressure changes in the liquid helium not only affect the cooling performance of the cavity but can also have a significant impact on its frequency stability. In particular, helium pressure fluctuations within the tank, especially in cryogenic environments, can lead to detuning of the cavity's frequency. This phenomenon is known as helium pressure fluctuation detuning.

Liquid helium fluctuations cause pressure variations within the helium tank, leading to surface deformation of the cavity, which in turn results in changes to the cavity's RF resonant frequency[24]. This deformation is directly proportional to the helium pressure fluctuations. The mathematical relationship between the cavity frequency and the helium pressure variation can be expressed as[25]:

$$\Delta f_1 = \frac{df}{dp} \times \Delta P \tag{1}$$

Here df/dp denotes the helium pressure sensitivity coefficient, which characterizes the sensitivity of the superconducting cavity to fluctuations in the helium bath pressure within the cryostat. ΔP represents the magnitude of the fluctuations in helium pressure.

C. Lorentz force detuning

Lorentz force detuning (LFD) arises from the inelastic deformation of the superconducting cavity material under the influence of a strong RF field[26]. The interaction between the RF field and the cavity material induces small deformations, particularly in the superconducting material (e.g., niobium). As the field strength increases, elastic deformation alters the geometry of the cavity, changing its RF resonant

frequency. The effect of the Lorentz force on an elliptical cavity is shown in Fig. 2[27]. When the accelerating gradient is $4.77\,\mathrm{MV/m}$, the Lorentz force distribution calculated by simulation is shown in the Fig. 3.

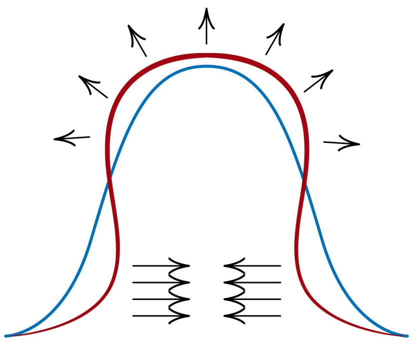

Fig. 2. Schematic of Lorentz force in an elliptical cavity. The blue contour denotes the original cell shape before deformation, the red blue contour denotes the deformed shape due to LFD.

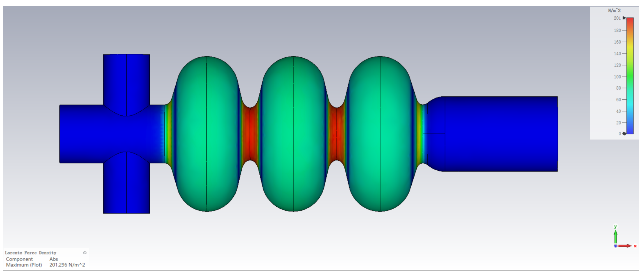

Fig. 3. Lorentz force distribution of the 3-cell superconducting cavity. When the accelerating gradient is $4.77\,\mathrm{MV/m}$, the Lorentz force is highest at the cavity iris, with a peak value of $201\,\mathrm{N/m^2}$.

The Lorentz force is generated by the electromagnetic field within the cavity and acts on the inner surface of the cavity, leading to deformation-induced detuning. The magnitude of the Lorentz force (P) is given by Equation[28]:

$$P = \frac{1}{4}(\mu_0 H^2 - \epsilon_0 E^2) \tag{2}$$

Here μ_0 is the vaccum permeability, ϵ_0 is the vaccum permittivity, and E and H are the magnetic field strength and electric field strength at the inner surface of the cavity, respectively.

Under different values of accelerating gradient E_{acc}, the deformation of the cavity and the corresponding frequency shift due to the Lorentz force vary. The frequency shift Δf is proportional to the square of the accelerating gradient E_{acc}^2:

$$\Delta f_2 = K_L \times E_{\text{acc}}^2 \tag{3}$$

Here K_L is Lorentz detuning coefficient. It represents the frequency effect of the Lorentz force detuning on the superconducting cavity.

For superconducting cavities in pulsed mode, LFD has a more significant impact, while helium pressure fluctuations are less influential[29, 30]. In contrast, for high-current ERL cavities in CW mode, Lorentz detuning primarily affects the early field buildup, so the focus is on mitigating the effect of helium pressure fluctuations, with Lorentz detuning as a secondary concern[31].

III. THE COMPLETE MODEL DETUNING ANALYSIS

Based on the internal profile parameters of the designed superconducting cavity[20], the cavity's outline can be sketched and modeled in CAD software. To minimize potential errors during the modeling process, the vacuum model established in the electromagnetic simulation phase is imported directly. Using the shell feature, the cavity's outer shell is automatically generated. The outer shell model is then precisely assembled with the vacuum model, effectively preventing interference issues in subsequent finite element analysis and ensuring the accuracy of the simulation.

The typical thickness for an $1.3\,\mathrm{GHz}$ superconducting cavity ranges from 2.5 to $3\,\mathrm{mm}$[32]. Insufficient thickness compromises the structural strength of the cavity, while excessive thickness could lead to challenges in welding and material waste. The thickness of the $1.3\,\mathrm{GHz}$ 3-cell high-current superconducting cavity is set to $2.8\,\mathrm{mm}$, which is similar to the TESLA cavity design[33]. The model of the dressed SRF cavity is shown in Fig. 4. The helium tank design and detailed parameters will be discussed in Chapter V.

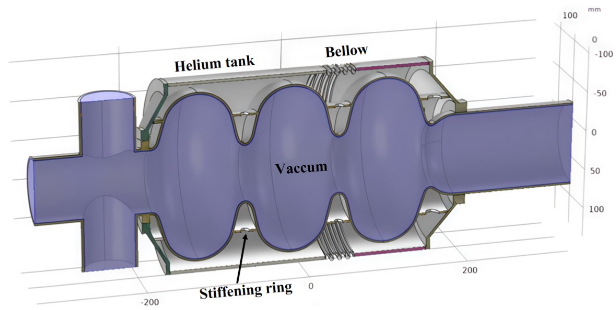

Fig. 4. Mechanical model (grey color) of 3-cell dressed SRF cavity with vacuum part (purple color) inside.

The elliptical cavity's relatively weak stiffness is one of its disadvantages. Therefore, an analysis of the detuning caused by helium pressure fluctuations, mechanical vibrations, and Lorentz forces is a necessary step in the development of the elliptical cavity. The accuracy of simulations largely depends on the precision of material properties. Given that the superconducting cavity involves multi-physics coupling of electromagnetic, mechanical, and thermal fields, various material properties must be considered. In electromagnetic field simulations, two primary materials are involved: Perfect electric conductor (PEC) and vacuum, with μ_0 set at 4×10^{-7} H/m and ϵ_0 set at 8.854×10^{-12} F/m. For the mechanical structural simulations, the mechanical properties of materials such

as niobium, niobium-titanium alloy, and titanium for the helium tank are required. The relevant mechanical properties of these materials, which can influence the cavity strength and stability, are summarized in Table1[34, 35].

Table 1. Properties of Superconducting Cavity Materials.

Performance parameters	Nb	Ti	Nb55Ti
Density $[kg/m^3]$	8570	4506	5700
Young's Modulus $[GPa]$	118	117	68
Poisson's Ratio	0.38	0.37	0.33
Allowable stress (S) in 4 K $[MPa]$	212.0	319.0	156.0
Allowable stress (S) in 293 K $[MPa]$	47.0	98.0	156.0

The helium pressure detuning (df/dp) of a 3-cell high-current superconducting cavity was simulated using COMSOL Multiphysics simulation software[36]. One end of the cavity's beam tube was fixed, while the other end was allowed to expand freely. A pressure of $1\,\mathrm{bar}$ was applied to both the external surface of the bare cavity and the inner surface of the helium tank to simulate pressure fluctuations within the dressed cavity. Meanwhile, in finite element analysis, parts with complex structures that have minimal impact on the simulation results should be appropriately optimized to save computational resources. For instance, the bellows with an intricate and convoluted design require a high mesh density to achieve its stiffness accurately. To optimize computational efficiency, this study employs a material stiffness parameter equivalence approach, replacing the actual bellows model with an equivalent straight pipe of the same length. This method preserves the original stiffness characteristics while significantly reducing mesh resource consumption. The simulation boundary condition and the equivalent straight pipe model are shown in Fig. 5.

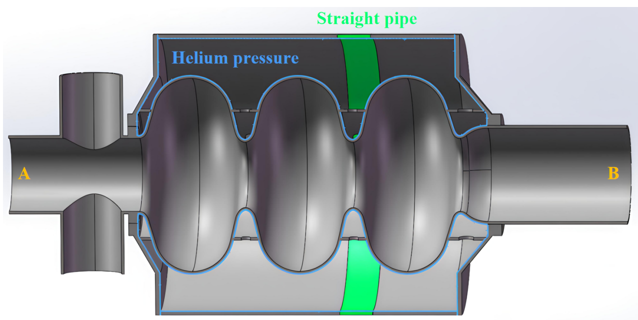

Fig. 5. A and B represent the beam tubes at both ends, helium pressure is inside helium vessel, and the green section represents the equivalent straight pipe model of the bellows.

The df/dp was evaluated as a function of the stiffening ring radius through multiphysics finite element simulations, with the analysis spanning three tuner stiffness conditions: $10\,\mathrm{kN/mm}$, $40\,\mathrm{kN/mm}$, and $80\,\mathrm{kN/mm}$. The simulation results are shown in Fig. 6. The outer diameter of the bare cavity iris is $38\,\mathrm{mm}$, and the outer diameter of the equator is 105 mm, so the range of possible stiffening ring radii is between $38\,\mathrm{mm}$ and $105\,\mathrm{mm}$, with $r_{ring} = 38\,\mathrm{mm}$ representing the case with no stiffening ring.

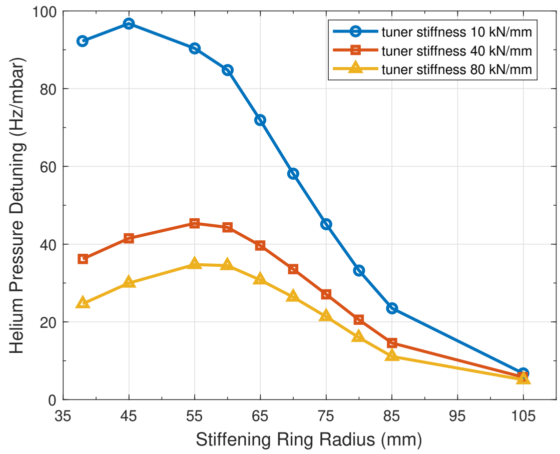

Fig. 6. df/dp of the 3-cell cavity for stiffening ring radii from 38 to $105\,\mathrm{mm}$ and tuner stiffnesses from 10 to $80\,\mathrm{kN/mm}$.

The helium pressure sensitivity initially increases with the stiffening ring radius and then begins to decrease significantly. In the TESLA cavity, the stiffening ring is located at the region where df/dp reaches its approximate maximum value. This is because the primary optimization goal for the stiffening ring in the TESLA cavity is to minimize Lorentz detuning rather than the microphone effect[37]. In contrast, when the stiffening ring is positioned at the equator, df/dp reaches its minimum. For a tuner stiffness of $40\,\mathrm{kN/mm}$[38], the optimal stiffening ring configuration to minimize df/dp was identified at the maximum radius position, followed by the configuration with no stiffening ring. For all stiffening ring radii, increasing the tuner stiffness results in a reduction of df/dp. This simulation provides a good assessment of the df/dp for the entire cavity, but it does not directly explain the variation of df/dp with stiffening ring radius and tuner stiffness, nor does it account for the influence of other specific components. Next, the factors influencing df/dp were analyzed and simulated individually.

IV. DECONSTRUCTIVE ANALYSIS AND VALIDATION OF HELIUM PRESSURE DETUNING

To investigate the factors contributing to the variation of df/dp in detail, the total frequency variation of the cavity is divided into two components: the frequency shift caused by changes in cavity length and the frequency shift resulting from changes in the shape of the cavity cells:

$$\Delta f_{total} = \Delta f_{\text{cell}} + \Delta f_{\text{length}} \tag{4}$$

Here Δf_{cell} is the frequency shift caused by the shape vari-

ations of the cavity cells, and Δf_{length} is the frequency shift caused by the cavity length change. The above equation divided by the change in helium pressure[39]:

$$\frac{df}{dp} = \frac{df_{\text{cell}}}{dp} + \frac{df_{\text{length}}}{dp} \tag{5}$$

The frequency shift Δf_{cell} results from the direct effect of liquid helium pressure on the outer wall of the cells. The helium bath pressure causes deformation of the cell walls.

The frequency shift Δf_{length} due to the cavity length change is attributed to the liquid helium's effect on the conical discs at both ends of the helium tank. The pressure from the helium bath exerts a stretching force at the ends, which leads to a change in the overall cavity length, thereby affecting the tuning of the cavity. The length variation can further be decomposed into two components: the original cavity length x and the force F applied to the cavity due to the elongation.

$$\frac{df_{\text{length}}}{dp} = \frac{df}{dx} \cdot \frac{dx}{dF} \cdot \frac{dF}{dp} = \frac{df}{dx} \cdot \frac{1}{K} \cdot \frac{dF}{dp} \tag{6}$$

Here df_{length}/dx represents the tuning sensitivity of the bare cavity, and K denotes the axial stiffness of the dressed cavity.

These parameters will be simulated and analyzed to evaluate the specific factors influencing df/dp. The simulation conditions for each parameter are listed in Table 2, and the corresponding loads applied can be seen in 5.

A. Helium pressure sensitivity of the bare cavity

First, the helium pressure detuning component Δf_{cell} is analyzed. In COMSOL, both ends of the beam pipe are fixed, and a pressure of 1 bar is applied to simulate the helium pressure acting solely on the outer wall of the bare cavity, to investigate the helium pressure detuning caused by the deformation of the cavity wall, denoted as df_{cell}/dp. The results are shown in Fig. 7.

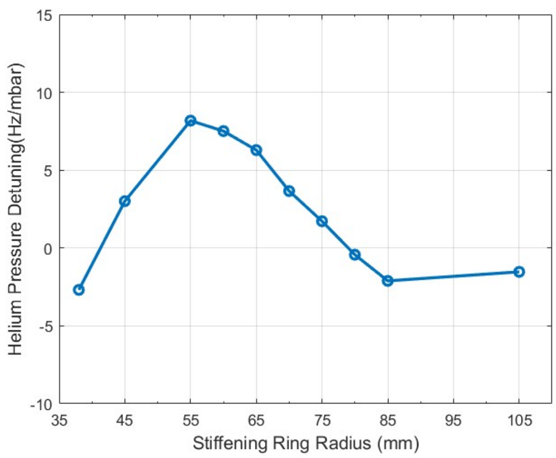

Fig. 7. df_{cell}/dp of cavity versus stiffening rings radius.

The results indicate that the variation in the bare cavity wall has a impact on df/dp, fluctuating between $-5\,\text{Hz/mabr}$ and $10\,\text{Hz/mbar}$. In the configuration without a stiffening ring, the df_{cell}/dp value is lower compared to the configuration with the stiffening ring placed at a radius of approximately $55\,\text{mm}$. This is because, as the helium pressure increases, the negative frequency shift caused by the deformation of the iris counteracts the positive frequency shift caused by the deformation of the equator and the increase in length.

B. The tuning sensitivity of the bare cavity

The tuning sensitivity df_{length}/dx of the bare cavity is influenced by the cavity shape and dimensions. Using COMSOL simulations, the relationship between the tuning sensitivity df_{length}/dx of the 3-cell cavity and the stiffening ring radius is simulated and presented in Fig. 8.

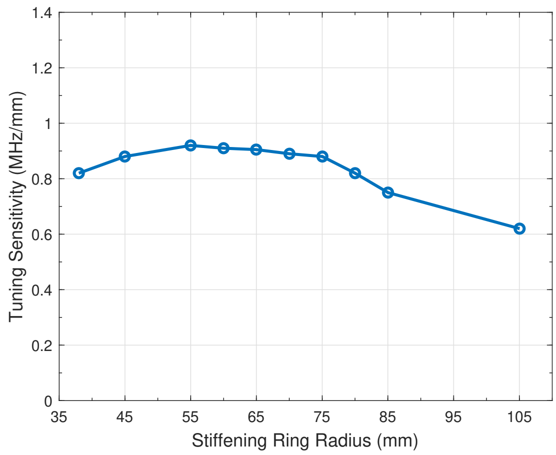

Fig. 8. Tuning sensitivity of cavity versus stiffening rings radius.

The results indicate that df_{length}/dx of the 3-cell superconducting cavity varies fractionally as the stiffening ring radius changes, fluctuating between $0.7\,\text{MHz/mm}$ and $1\,\text{MHz/mm}$. Overall, the stiffening ring radius does have some effect on df_{length}/dx, but this influence is relatively small.

C. Axial stiffness and helium pressure tuning force

The cavity axial stiffness is an essential factor in the study of helium pressure detuning. Stiffness simulations were conducted for both the bare cavity and the dressed cavity, with the comparative results presented in Fig. 9.

In addition to exerting pressure on the cavity walls, the liquid helium in the helium bath also induces deformation of the bath wall itself due to the pressure, thereby generating a tensile force in the axial direction on the cavity. For the 3-cell cavity, the pressure on the end wall of the helium bath has the most significant impact on the dF/dp. As shown in

Table 2. Simulations for determining df/dp model parameters.

Parameter	Boundary conditions	Load	Calculation results
df_{cell}/dp	A, B tubes fixed	1 bar helium pressure	frequency variation
df_{length}/dx	A tube fixed	1 mm displacement (B)	frequency variation
K	A tube fixed	2.5 kN axial force (B)	Length change
dF/dp	A, B tubes fixed	1 bar helium pressure	Average force

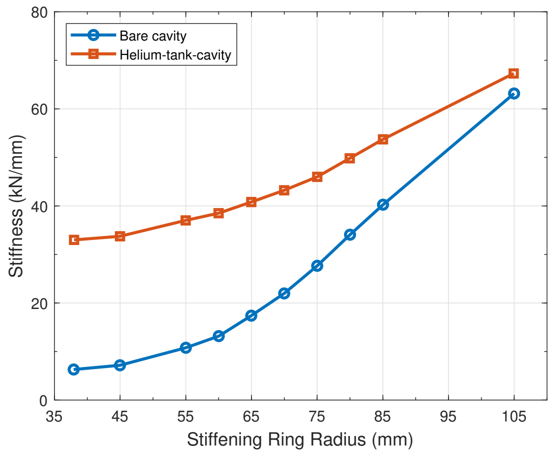

Fig. 9. Stiffness of bare cavity and dressed cavity versus stiffening rings radius.

Fig. 10, for a cavity with a stiffening ring radius of 70 mm as an example, the pressure applied on the end wall of the helium bath, which has a small outer diameter of 120 mm, was simulated and integrated in COMSOL to calculate the resulting force. When the internal pressure was 1 bar, the integral result of the force component in the x-direction (axial direction), dp_{x}, was 3499.4 N. Therefore, for the 3-cell cavity, $dF/dp = 3499.4$ N/bar.

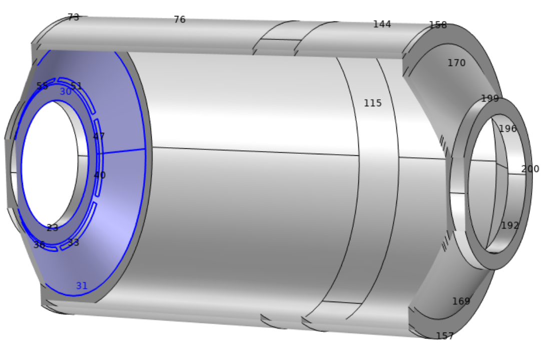

Fig. 10. Integral region of pressure on the helium tank end wall.

To further investigate the effect of helium pressure on the end wall of the helium bath on df/dp, a cavity model with an end wall outer diameter expanded to 150 mm was established, while keeping other parameters unchanged. The integral result of the force component dp_{x} was 6023.3 N. The detuning simulation results are shown in Table 3. It can be observed that as the outer diameter of the helium bath's end wall increases, the df/dp of the cavity rises rapidly.

Table 3. Simulation comparison of dressed cavities with different outer diameters for stiffening rings radius of 70 mm.

Detuning	120 mm	150 mm
df/dp@ K_{tuner}10 kN/mm	58.07	114.73
df/dp@ K_{tuner}40 kN/mm	33.49	95.10
df/dp@ K_{tuner}80 kN/mm	26.32	90.79

The main source of the cavity length change caused by helium pressure is the pressure exerted by the helium bath on the end walls of the helium tank. When using the same type of tuner, the ratio of dF/dp for different cavities is approximately equal to the ratio of the endwall areas of the helium bath. Therefore, reducing the diameter of the helium bath is a feasible approach to optimize helium pressure detuning[40, 41].

D. Summary of helium pressure sensitivity model

Building on the previous simulations, an independent analysis was conducted for each influencing factor outlined in Eq. (6), and the impact of each factor was quantified through simulation. Fig. 11 shows the results of df_{length}/dp under the condition of a tuner stiffness of 40 kN/mm. Furthermore, the influence of cell cavity wall deformation, df_{cell}/dp, is also plotted. The sum of these two components is compared with the complete simulation result of df/dp for the entire cavity[39].

The decomposition prediction of the model is in close agreement with the complete simulation of the entire cavity. The difference between the two is less than 5% at most of the data points, validating the reliability of the helium pressure detuning model and its conclusions. Therefore, increasing K, or reducing df_{cell}/dp, tuning sensitivity k_{tune}, or helium tank end-wall area S, are all effective methods to reduce df/dp.

For the 3-cell cavity without a stiffening ring, the impact of cavity wall deformation on frequency is relatively small. This

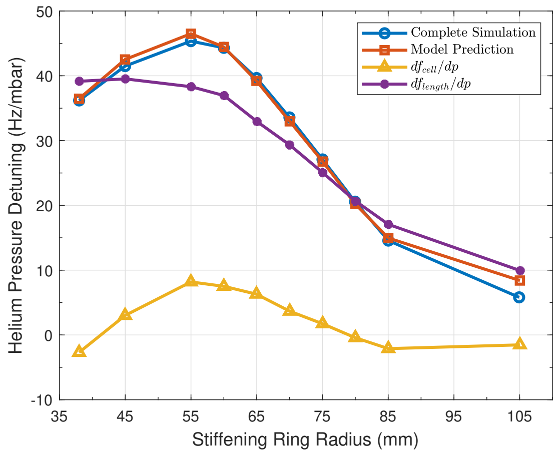

Fig. 11. Comparison of model combinations and complete cavity simulations. df_{cell}/dp is the frequency shift caused by the shape variations of the cavity cells, and df_{length}/dp is the frequency shift caused by the cavity length change. The combined model result is derived by formulating the individual simulation results from above, and it closely matches the curve obtained from the completed dressed cavity simulation.

is because the positive frequency shift caused by the equatorial deformation counteracts the negative frequency shift caused by the iris deformation[42]. For the 3-cell cavity with the stiffening ring, the stiffening ring changes the balance. And the stiffening ring changes the stiffness K and limits the deformation of the bare cavity, thereby affecting df_{length}/dp and df_{cell}/dp.

When selecting the location of the stiffening ring, multiple factors need to be considered. The cavity's strength cannot be too weak, so a stiffening ring is required to ensure its structural integrity. If the stiffening ring radius of the cavity is set in the region where df/dp is relatively low, meaning the stiffening ring radius is larger, this effectively reduces the detuning caused by helium pressure variations. However, it also results in greater tuning difficulty. Therefore, after balancing the reduction of df/dp with tuning flexibility, this study preliminarily sets the stiffening ring radius at $70\,\text{mm}$ to optimize the performance of the superconducting cavity.

V. MECHANICAL STRUCTURE ANALYSIS

Building upon the findings from the previous chapter, the fundamental structural parameters of the superconducting cavity are further refined. The thickness of the bare cavity wall is set at $2.8\,\text{mm}$, and the stiffening ring radius is established at $70\,\text{mm}$ to enhance the structural stability. Additionally, to ensure the deformation consistency between the end cell and the middle cell during tuning, a stiffening ring is also installed at the position of the U-shaped beam pipe. The thickness of the stiffening ring is set to $3\,\text{mm}$, and to maintain helium flow, six evenly distributed holes are placed on the stiffening ring. The hole diameter between the cells is set to $10\,\text{mm}$, while the holes connecting the end cells and the U-shaped beam pipe are larger, with a diameter of $16\,\text{mm}$. Fig. 12 shows the sectional view of the bare cavity.

This study also includes an in-depth investigation of the mechanical performance of the $1.3\,\text{GHz}$ superconducting cavity, covering the simulation of the tuning force and microphonics, the analysis of the Lorentz force detuning and the evaluation of the pressure tolerance.

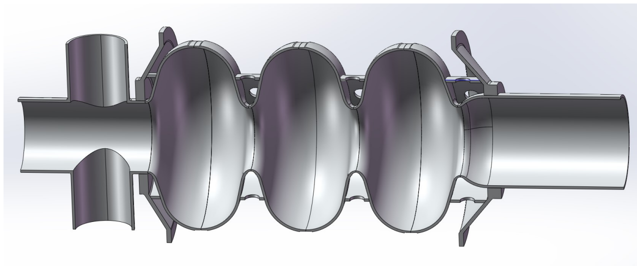

Fig. 12. Cross-sectional view of the bare cavity with a $70\,\text{mm}$ stiffening ring radius, highlighting the structural configuration.

A. The analysis of the tuning force

In the cryomodule, the frequency fine-tuning of the superconducting cavity is achieved through a precise piezo tuner. However, before the cavity is assembled into the cryomodule, coarse frequency tuning must be performed using a mechanical tuner. For an $1.3\,\text{GHz}$ superconducting cavity, the typical tuning range is $500\,\text{kHz}$[43]. To ensure that the cavity is not damaged within the tuning range, it is necessary to simulate the force required for a $500\,\text{kHz}$ frequency shift during the tuning process.

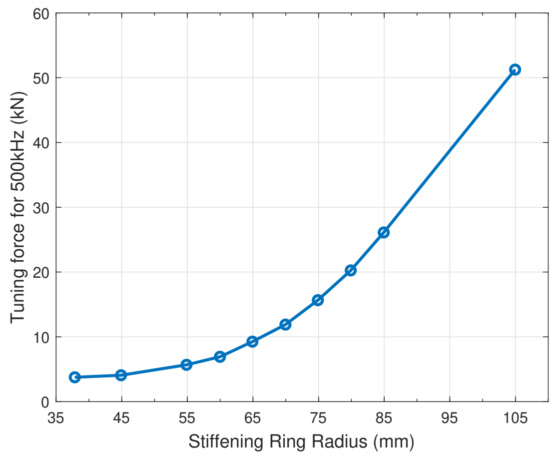

Fig. 13. Tuning force for $500\,\text{kHz}$ versus stiffening rings radius.

The force required to tune a frequency shift of $500\,\text{kHz}$ in the 3-cell superconducting cavity as a function of the stiffening ring radius is shown in Fig. 13. The results indicate

that as the radius of the stiffening ring increases, the required tuning force rises exponentially. When the radius exceeds 85 mm, the tuning force becomes very large (greater than 30 kN), which poses significant challenges for the tuner design. Therefore, the cavity with a 70 mm stiffening ring radius demonstrated compliance with operational specifications, while the required tuning force of less than 15 kN significantly reduced mechanical adjustment complexity and simplified the tuner design requirement.

B. The analysis of microphonics

The microphone effect is closely related to the mechanical vibration modes of the superconducting cavity. When the cavity's natural mechanical modes are influenced by external vibrations, it can trigger mechanical vibrations within the superconducting cavity, sometimes causing detuning of the RF resonant frequency. The structure of the superconducting cavity has a specific response pattern to external disturbances, with mechanical vibrations being transmitted to the cavity through transmission lines, low-temperature systems, supports, and the ground. When the frequency of the external vibration matches the inherent mechanical resonance frequency of the cavity, mechanical resonance can occur, leading to deformation of the cavity and subsequently affecting the stability of the RF resonant frequency. To ensure the stable operation of the superconducting cavity and prevent low-frequency resonance caused by environmental vibrations, it is crucial to understand and enhance the intrinsic vibration frequency of the cavity.

Based on this, a modal analysis was performed on an 1.3 GHz superconducting cavity with stiffening rings radius of 70 mm, and the simulation results are shown in Fig. 14. Additionally, the modal analysis results for the cavity without the stiffening ring and the cavity with 70 mm stiffening ring are presented in Table 4. The results indicate that even without the stiffening ring, the lowest modal frequency of the cavity reaches 199.58 Hz, which is significantly higher than the typical vibration frequency of 100 Hz commonly observed in standard equipment[44]. This demonstrates that the cavity's vibration modes meet the design requirements.

Table 4. Mechanical modes of 3-cell superconducting cavity.

	w/o stiffening ring	70 mm stiffening ring
Mode 1 [Hz]	199.58	266.43
Mode 2 [Hz]	205.66	299.36
Mode 3 [Hz]	339.88	449.16
Mode 4 [Hz]	357.76	513.51
Mode 5 [Hz]	403.96	619.58
Mode 6 [Hz]	478.29	735.89

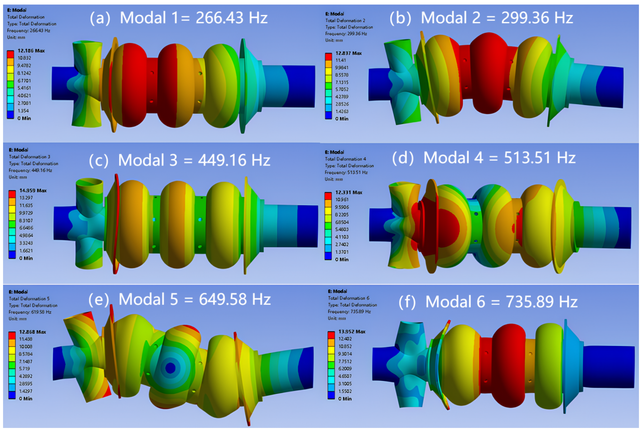

Fig. 14. The lowest six mechanical modes of the cavity with stiffening rings. For the cavity with a 70 mm radius and a stiffening ring, the lowest natural mechanical frequencies of (a) Mode 1 and (b) Mode 2 are significantly higher than 50 Hz.

C. The analysis of Lorentz force detuning

In the CW operation of the ERL high-current superconducting cavity, Lorentz detuning primarily affects the cavity during the initial field buildup phase. Simulation results are shown in Fig .15, under the design accelerating gradient of 12 MV/m and a tuner stiffness of 40 kN/mm, the frequency shift caused by Lorentz forces ranges between 138 Hz and 197 Hz. The 70 mm stiffening ring radius is optimized for minimizing df/dp, and at this point, the superconducting cavity exhibits a relatively high Lorentz detuning coefficient, with a detuning amount of 162 Hz. Despite the relatively large detuning, this does not imply that the cavity cannot operate normally. By employing feedforward control, the effects of Lorentz detuning can be effectively compensated and eliminated[45, 46].

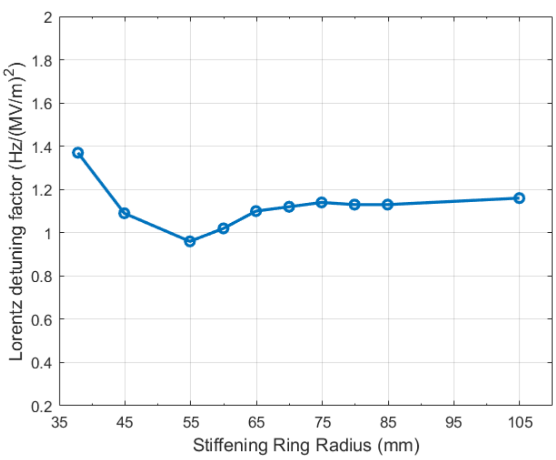

Fig. 15. Lorentz detuning factor of cavity versus stiffening rings radius.

Feedforward control is a technique that preemptively compensates for detuning before it occurs. The feedforward con-

Table 5. Summary of Stress Analysis Results Under Different Working Conditions

Condition	Loads	Boundary	Temperature	Peak Stress on Cavity	Allowable Stress
Leak check (bare cavity)	i) Gravity ii) $P_1 = 0$ iii) $P_2 = P_3 = 0.1$ MPa	Both ends fixed	293 K	5.30	47.0 (S) 70.5 (1.5S)
Vertical test (bare cavity)	i) Gravity ii) $P_1 = 0$ iii) $P_2 = P_3 = 0.15$ MPa	Both ends fixed	4.2 K	7.95	212 (S) 318 (1.5S)
Horizontal test (dressed cavity)	i) Gravity ii) $P_1 = P_3 = 0$ iii) $P_2 = 0.2$ MPa	Single-end fixed	4.2 K	18.4	212 (S) 318 (1.5S)
Extreme situation (dressed cavity)	i) Gravity ii) $P_1 = P_3 = 0$ iii) $P_2 = 0.225$ MPa	Single-end fixed	4.2 K	20.6	212 (S) 318 (1.5S)

trol system continuously monitors the cavity's operational parameters through sensors, predicts the potential detuning, and generates corresponding corrective signals. These signals are then used to adjust the tuner, temperature control, or power supply systems to immediately correct the frequency shift[47]. In this way, feedforward control allows for proactive measures to maintain frequency stability before detuning occurs. This control method is particularly suitable for CW operation, which requires high stability, as it ensures the cavity's frequency remains stable without interfering with the acceleration process, thus preventing performance degradation due to frequency shifts[48].

D. The analysis of stress under different loading conditions

As mentioned in previous conclusions, a smaller helium vessel diameter positively impacts the reduction of df/dp, thus the diameter of the helium vessel is designed to be as small as possible. To avoid interference between the bellows and the bare cavity, considering the outer diameter of the bare cavity is $106\,\mathrm{mm}$, the inner diameter of the helium vessel was set to 116 mm, with a wall thickness of $4\,\mathrm{mm}$. The INFN blade tuner is selected, with the bellows positioned at the center of the helium vessel. While this layout compromises the strength of the helium tank due to the presence of the bellows, it eliminates the need for additional longitudinal clearance, allowing for effective space savings[49–51]. The cavity model with a helium tank and bellows is shown in Fig .16.

The purpose of the stress analysis is to ensure that the mechanical design of the superconducting cavity can withstand the most challenging conditions encountered during its fabrication, testing, and operation. A comprehensive stress analysis of the dressed cavity was performed under four distinct loading conditions, including the effects of the helium vessel and gravity. The loading scenarios examined include leak tests, vertical tests, horizontal testing at cryogenic temperature, and extreme situation. The allowable stress limits for each material at room temperature and cryogenic temperatures are provided in Table 1. Based on the simulation results, the calculated stresses for all four loading conditions are within the permissible safety thresholds[52], P_1 is inside cavity, P_2 is inside helium vessel and P_3 is outside helium vessel, as summarized in Table 5, confirming that the cavity meets the stress safety criteria for operation. The stress distribution under vertical test is shown in Fig .17. The maximum stress in the cavity is much lower than the material's allowable stress, and the cavity meets the strength requirements for

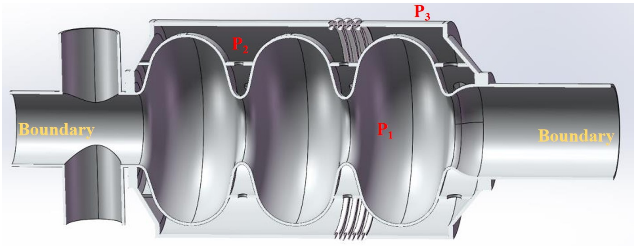

Fig. 16. Schematic of 3-cell cavity helium tank with bellows. Red area represents the loads of the stress analysis, and the yellow area represents the boundary conditions.

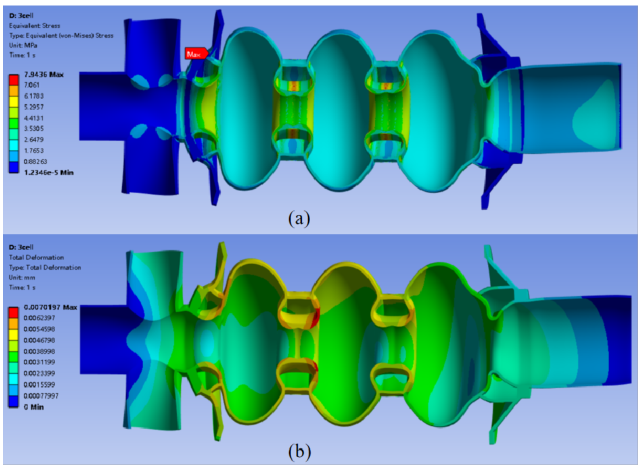

Fig. 17. (a) Stress and (b) deformation of the cavity under vertical test. Boundary and loading conditions depicted in Fig. 16 are used.

stable operation under vertical test.

VI. CONCLUSION

This study presents a comprehensive simulation and analysis methodology for helium pressure-induced detuning in high-current ERL superconducting cavities and structural optimizations to ensure long-term frequency and mechanical stability. A detailed investigation into the detuning mechanisms of the 1.3 GHz 3-cell injector cavity was conducted, utilizing multiphysics simulations to analyze the factors influencing helium pressure detuning. A predictive model for helium pressure detuning was established. To ensure stable operation of the superconducting cavity, the stiffening ring position was optimized to 70 mm. This modification significantly mitigated the impact of helium pressure detuning, reducing the frequency shift caused by helium bath pressure variations from $45.3\,\mathrm{Hz/mbar}$ to $33.4\,\mathrm{Hz/mbar}$, with a peak detuning of 10 Hz. Additionally, this design avoids the tuning challenges associated with the excessively large stiffening ring radius, achieving a tuning range of 500 kHz with a tuning force of less than 15 kN, which significantly improves operational feasibility. Furthermore, critical structural components of the cavity were optimized, and their performance was rigorously evaluated. The optimized design demonstrated excellent results in stiffness, strength, and modal analysis, ensuring robust structural stability.

In summary, this paper provides a thorough analysis and design optimization of the mechanical structure of the 1.3 GHz 3-cell high-current superconducting cavity, significantly enhancing its frequency stability and mechanical performance. These advancements ensure its suitability for continuous-wave, high-β, and high-current operation in ERL applications. The findings offer a valuable reference for the mechanical design of superconducting cavities, contributing to the development of more efficient and stable accelerator systems.

VII. ACKNOWLEDGEMENTS

This work was supported by the National Natural Science Foundation of China (12125508), the National Key Research and Development Program of China (2024YFA1612104), the CAS Project for Young Scientists in Basic Research (YSBR-042), and Shanghai Pilot Program for Basic Research – Chinese Academy of Sciences, Shanghai Branch (JCYJ-SHFY-2021-010).

VIII. REFERENCES

[1] Wataru M., Shigeru S. Fundamentals of Synchrotron Radiation Science[M]. Fundamentals of Synchrotron Radiation Science, 2010, doi: 10.5772/intechopen.82202.

[2] Ciovati G, Cheng G, Daly E, et al. Cavity Production and Testing of the First C75 Cryomodule for CEBAF[C]. 2022, doi: 10.18429/JACoW-SRF2021-MOPCAV001.

[3] Adolphsen C, Andre K, Angal-Kalinin D, et al. The development of energy-recovery linacs[J]. arXiv preprint arXiv:2207.02095, 2022,doi: 10.48550/arXiv.2207.02095.

[4] Bartnik A, Hoffstaetter G H, Banerjee N, et al. CBETA: First Multipass Superconducting Linear Accelerator with Energy Recovery[J]. Phys. Rev. Lett., 2020, 125(4): 044803.

[5] Hoffstaetter G H, Bazarov I V, Berg J S, et al. CBETA Design Report, Cornell-BNL ERL Test Accelerator[R]. arXiv: 1706.04245.

[6] Obina T, Hara K, Seimiya Y, et al. 1 mA Stable Energy Recovery Beam Operation with Small Beam Emittance[C]. 2019, doi: 10.18429/JACoW-IPAC2019-TUPGW036.

[7] Watanabe K, Noguchi S, Kako E, et al. Development of the superconducting RF 2-cell cavity for cERL injector at KEK[J]. Nucl. Instrum. Methods Phys. Res. Sect. A, 2013, 714: 67–82.

[8] Steinhorst M, Arnold M, Bahlo T, et al. LOW LEVEL RF ERL EXPERIENCE AT THE S-DALINAC[C]//Proc. 63rd Advanced ICFA Beam Dynamics Workshop on Energy Recovery Linacs (ERL'19). 2020: 52-55, doi: 10.18429/JACoW-ERL2019-TUCOZBS05.

[9] Stengler T, Aulenbacher K, Hug F, et al. Cryomodules for the Mainz Energy-Recovering Superconducting Accelerator (MESA)[C]//63th ICFA Advanced Beam Dynamics Workshop on Energy Recovery Linacs ERL. 2019, doi: 10.18429/JACoW-ERL2019-TUCOZBS06.

[10] Kaabi W, Stocchi A, Bogacz A, et al. PERLE: A novel facility for ERL development and applications in multi-turn configuration and high-power regime[C]//29th Cracow Epiphany Conference on Physics at the Electron-Ion Collider and Future Facilities. 2023, 16(7): 7-A21. https://www.osti.gov/biblio/2274942

[11] Méot F, Ben-Zvi I, Hao Y, et al. ER@ CEBAF-A 7 GeV, 5-Pass, Energy Recovery Experiment[C]//59th ICFA Advanced Beam Dynamics Workshop on Energy Recovery Linacs (ERL'17), Geneva, Switzerland, June 18–23, 2017. JACoW Publishing, Geneva, Switzerland, 2018: 58–58, https://www.osti.gov/biblio/1392263.

[12] Montag C, Zaltsman A, Blednykh A, et al. The EIC accelerator: design highlights and project status[R]. Lawrence Berkeley National Laboratory (LBNL), Berkeley, CA (United States); Fermi National Accelerator Laboratory (FNAL), Batavia, IL (United States); Oak Ridge National Laboratory (ORNL), Oak Ridge, TN (United States); Brookhaven National Laboratory (BNL), Upton, NY (United States); SLAC National Accelerator Laboratory (SLAC), Menlo Park, CA (United States); Thomas Jefferson National Accelerator Facility (TJNAF), Newport News, VA (United States), 2024, doi: 10.18429/JACoW-IPAC2024-MOPC67.

[13] Chen, JF., Zong, Y., Pu, XY. et al. Ultra-high quality factor and ultra-high accelerating gradient achievements in a 1.3 GHz continuous wave cryomodule. NUCL SCI TECH 36, 25 (2025), doi: 10.1007/s41365-024-01630-y.

[14] Pan W, Zhai J, He F, et al. High Q and high gradient performance of the first medium-temperature baking 1.3 GHz cryomodule[J]. Physical Review Accelerators and Beams, 2024, 27(9): 092003. DOI10.1103/PhysRevAccelBeams.27.092003.

[15] He F, Pan W, Sha P, et al. Medium-temperature furnace baking of 1.3 GHz 9-cell superconducting cavities at IHEP[J]. Superconductor Science and Technology, 2021, 34(9): 095005. https://api.semanticscholar.org/CorpusID:236942829.

[16] Zong Y, Chen J, Wang D, et al. Investigation of Electropolishing for High-Gradient 1.3 GHz and 3.9 GHz Niobium Cavities[J]. Materials, 2024, 17(13): 3207. doi: 10.3390/ma17133207.

[17] Zong Y, Chen J F, Wang D, et al. Accelerating gradient improvement in nitrogen-doped superconducting radio-frequency cavities for SHINE[J]. Nuclear Instruments and Methods in Physics Research Section A: Accelerators, Spectrometers, Detectors and Associated Equipment, 2023, 1057: 168724. doi: 10.1016/j.nima.2023.168724.

[18] Pan W, Ge R, Li M, et al. Cryogenic system of the high performance 1.3 GHz 9-cell superconducting radio frequency prototype cryomodule[J]. Applied Thermal Engineering, 2024, 255: 124042. doi: 10.1016/j.applthermaleng.2024.124042.

[19] N. Huang, H. Deng, B. Liu et al., Features and futures of X-ray free-electron lasers. Innovation 2, 100097 (2021). doi: 10.1016/j.xinn.2021.100097

[20] Xuan Huang, 1.3 GHz 3-cell superconducting cavity for high current beam acceleration, paper presented at the 69th ICFA Advanced Beam Dynamics Workshop on Energy Recovery Linacs, KEK, Tsukuba, Japan, https://conference-indico.kek.jp/event/225/contributions/5564/attachments/3919/5363/THO16.pdf, 24-27 September 2024

[21] Chen X, Liu Z, Chen S, et al. The design of high-brightness ERL-FEL injector based on VHF electron gun[J]. Nucl. Instrum. Methods Phys. Res. Sect. A, 2025, 1070: 170058.

[22] Aizaz A, Grimm T L, Wright N T. Thermal design studies in superconducting RF cavities: Phonon peak and Kapitza conductance[J]. Phys. Rev. Accel. Beams, 2010, 13(9): 093503.

[23] Neil G R, Bohn C L, Benson S V, et al. Sustained Kilowatt Lasing in a Free-Electron Laser with Same-Cell Energy Recovery[J]. Phys. Rev. Lett., 2000, 84(4): 662–665.

[24] Lin M C, Wang C, Chang L H, et al. Effects of Structural Behavior on Electromagnetic Resonance Frequency of a Superconducting Radio Frequency Cavity[J]. J. Mech., 2007, 23(3): 187–196, doi: 10.1017/S1727719100001210.

[25] Fan P, Zhu F, Zhong H, et al. Mechanical analysis of low 162.5 MHz taper HWR cavity[J]. High Power Laser Part. Beams, 2016, 28: 045103. doi: 10.11884/HPLPB201628.125103.

[26] Rathore M, Jain V K, Atulkar A, et al. Study of Lorentz force detuning and its compensation in superconducting radiofrequency cavity: a review[J]. Materials Today: Proceedings, 2021, 44: 1369-1374.doi: 10.1016/j.matpr.2020.11.506.

[27] Rathore M, Jain V K, Singh K K, et al. Estimation of Lorentz force detuning and its compensation on 650 MHz single-cell SCRF cavity[J]. Eng. Res. Express, 2021, 3(2): 025025, doi: 10.1088/2631-8695/abfdf7.

[28] Awida M H, Gonin I, Passarelli D, et al. Multiphysics analysis of frequency detuning in superconducting RF cavities for proton particle accelerators[C]//2015 IEEE MTT-S International Conference on Numerical Electromagnetic and Multiphysics Modeling and Optimization (NEMO). 2015: 1–3., https://www.osti.gov/biblio/1247523

[29] MITCHELL R, MATSUMOTO K, CIOVATI G, et al. Lorentz Force Detuning Analysis of the Spallation Neutron Source(SNS) Accelerating Cavities[C]. Proceedings of the 10th Workshop on RF Superconducty, 200: 236.https://api.semanticscholar.org/CorpusID:54492898

[30] CARCAGNO R, BRANLARD J, CHASE B, et al. First Fermilab Results of SRF Cavity Lorentz Force Detuning Compensation Using a Piezo Tuner[C]. Proceedings of SRF2007, https://api.semanticscholar.org/CorpusID:59137803, 2007: 259.

[31] Verdú-Andrés S, Belomestnykh S, Wu Q, et al. Lorentz detuning for a double-quarter wave cavity[J]. 2015, doi: 10.18429/JACOW-SRF2015-THPB051.

[32] Zvyagintsev V, Beard C D, Grassellino A, et al. Nine-cell elliptical cavity development at TRIUMF[C]//Proceedings SRF 2011 Conference, Chicago, IL. ,https://accelconf.web.cern.ch/SRF2011/papers/mopo020.pdf, 2011.

[33] Aune B, Bandelmann R, Bloess D, et al. Superconducting TESLA cavities[J]. Phys. Rev. Accel. Beams, 2000, 3(9): 092001.

[34] Mario M. Material properties for engineering analyses of SRF cavities[R]. Fermilab Specification 5500.000-ES-371110, https://accelconf.web.cern.ch/ipac2017/papers/mopva114.pdf, 2011.

[35] ASME. ASME Boiler and Pressure Vessel Code Section II Materials[R]. ASME, https://cdn.asme.org/getmedia/f40d9134-6941-41ac-9cc8-a7022a890b72/34011.pdf,2010.

[36] COMSOL Multiphysics®. Ver. 5.3a, COMSOL Co., Ltd., https://cn.comsol.com/.

[37] Simrock S N. Lorentz force compensation of pulsed SRF cavities[C]//Proceedings of LINAC. 2002, 2002: 555.

[38] Contreras-Martinez C, Pischalnikov Y, Yun J C. Simulated Lorentz Force Detuning Compensation With A Double Lever Tuner On A Dressed ILC/1.3 GHz Cavity At Room Temperature[J]. arXiv preprint arXiv:2208.06286, 2022.

[39] Edwards D A, et al. TESLA Test Facility Linac Design Report[R]. DESY, Chap. 4, 1995.

[40] Zaplatin E, et al. In Proceedings of the 10th European Particle Accelerator Conference, Edinburgh, Scotland, 2006 (Ref. [21]), MOPCH157.

[41] Zaplatin E. PAC 2011, New York, NY (Ref. [1]), TUP031.

[42] Posen S, Liepe M. Mechanical optimization of superconducting cavities in continuous wave operation[J]. Phys. Rev. Accel. Beams, 2012, 15(2): 022002.

[43] Pu X Y, Hou H T, Wang Y, et al. Frequency sensitivity of the passive third harmonic superconducting cavity for SSRF[J]. Nuclear Science and Techniques, 2020, 31(3): 31.

[44] Zhang X, Sha P, Pan W, et al. The mechanical design, fabrication and tests of dressed 650 MHz 2-cell superconducting cavities for CEPC[J]. Nucl. Instrum. Methods Phys. Res. Sect. A, 2022, 1031: 166590.

[45] Bo X., Liu H., Wang Y., et al. Study on Detuning of Superconducting Elliptical Cavities in CSNS-II[J]. Chinese Journal of Nuclear Physics Review, 2020, 37(2).

[46] MITCHELL R, MATSUMOTO K, CIOVATI G, et al. Lorentz Force Detuning Analysis of the Spallation Neutron Source (SNS) Accelerating Cavities[C]//Proceedings of the 10th Workshop on RF Superconductivity, 200: 236.

[47] DEVANZ G, BAZIN N, DESMONS P, et al. ESS Elliptical Cavities and Cryomodules[C]//Proceedings of SRF2013, 2013: 1218.
[48] CARCAGNO R, BRANLARD J, CHASE B, et al. First Fermilab Results of SRF Cavity Lorentz Force Detuning Compensation Using a Piezo Tuner[C]//Proceedings of SRF2007, 2007: 259.
[49] Solyak N, Borissov E, Gonin I, et al. SRF cavity tuning for low beam loading[C]//Proc. SRF. 2013: 1110–1114.
[50] Pagani, Carlo, et al. Improvement of the blade tuner design for superconducting RF cavities. Proceedings of the 2005 Particle Accelerator Conference. IEEE, 2005.
[51] Solyak, N., et al. SRF cavity tuning for low beam loading. Proc. SRF. 2013.
[52] Zheng H, Zhang P, Li Z, et al. Design optimization of a mechanically improved $499.8\,\mathrm{MHz}$ single-cell superconducting cavity for HEPS[J]. IEEE Trans. Appl. Supercond., 2020, 31(2): 1–9.